PHYSICAL REVIEW D **96,** 015009 (2017)

Longitudinal W boson scattering in a light scalar top scenario

Koji Ishiwata and Yuki Yonekura

Institute for Theoretical Physics, Kanazawa University, Kanazawa 920-1192, Japan

(Received 24 March 2017; published 11 July 2017)

Scalar tops in the supersymmetric model affect the potential of the standard model-like Higgs at the quantum level. In light of the equivalence theorem, the deviation of the potential from the standard model can be traced by longitudinal gauge bosons. In this work, high-energy longitudinal W boson scattering is studied in a TeV-scale scalar top scenario. $\mathcal{O}(1$–$10\%)$ deviation from the standard model prediction in the differential cross section is found, depending on whether the observed Higgs mass is explained only by scalar tops or by additional contributions at a higher scale.

DOI: 10.1103/PhysRevD.96.015009

I. INTRODUCTION

The recent discovery of the Higgs boson confirmed the standard model (SM) of particle physics [1,2]. Since then, Higgs properties have been measured at the LHC and found to be consistent with the standard model prediction [3]; besides, there has been no sign beyond the standard model in the experiment. It is widely believed, however, that the standard model is not the ultimate theory. Superstring theory is one of candidates for the "theory of everything." It requires supersymmetry (SUSY) due to consistency, which gives rise to lots of phenomenological consequences beyond the standard model. For example, it provides a candidate for dark matter, and three gauge coupling constants are unified at the grand unification scale. Supersymmetry affects the Higgs sector, too. In SUSY, another Higgs doublet must be introduced for the phenomenologically acceptable Higgs mechanism to work. In the supersymmetric Higgs sector, the electroweak symmetry breaking (EWSB) is induced by renormalization flow of parameters in the Higgs sector, which is a solution to the origin of the EWSB since in the SM it is induced by the *ad hoc* tachyonic Higgs mass term. In spite of such a drastic extension, the Higgs sector in the supersymmetric model reduces to the one in the SM below the electroweak scale when superpartners are much heavier than the electroweak scale. Considering the current status, i.e., no sign of a new particle so far, this might be the case, and then it might be difficult to observe a clue of supersymmetry even in future collider experiments.

In such a circumstance, it is worth recalling that the observed 125 GeV Higgs mass cannot be explained in SUSY at tree level. It is explained by scalar top ("stop") loop contribution, for example, in the minimal supersymmetric standard model (MSSM) [4–9]. This fact indicates that the stop has an impact on the SM Higgs potential at the quantum level, which is similar to the Higgs sector in classical scale-invariant model. In a simple classical scale-invariant model, (a) SM singlet scalar(s) is (are) introduced. They affect the Higgs potential at the quantum level, which induces the EWSB radiatively. In this framework, the singlet loop determines the curvature of the Higgs potential around the minimum, i.e., the Higgs mass. Although Higgs properties, such as mass, production, and decay rates at collider experiments, are almost consistent with the SM values, the Higgs self-couplings are predicted to significantly deviate from the SM ones [10–12]. This means that Higgs potential is the same locally around the minimum but not in a global picture. Such an effect is imprinted in fictitious bosons in the Higgs doublet, which are absorbed into longitudinal polarization of the gauge bosons. While the measurement of the Higgs self-couplings is one of main goals of the next-generation lepton collider, e.g., the International Linear Collider (ILC), the deviation from the SM in the Higgs sector can be also probed at the LHC in the gauge boson scattering process. It is pointed out in Ref. [13] that the differential cross sections of longitudinal gauge boson scattering processes $W_L^+W_L^+ \to W_L^+W_L^+$ and $W_L^+W_L^- \to W_L^+W_L^-$ are changed by more than $\mathcal{O}(10\%)$ in the model, which is described by off-shell Higgs. Namely, the discrepancy between the classical scale-invariant model and the SM can be found in off-shell Higgs in the propagator, for which the longitudinal gauge boson scattering is a good probe.

In the supersymmetric model, stops are expected to play a role similar to the singlet scalars. In this paper, we analyze the longitudinal gauge boson scattering in the framework of the supersymmetric model. Following the analysis in Ref. [13], we formulate the leading-order amplitudes of the processes and discuss the deviation from the standard model prediction numerically.

In the study, we consider stops with a mass of less than a few TeV. Such a light stop scenario is motivated by the naturalness argument, and part of parameter space of the scenario has already been excluded by the direct search at the LHC. In Ref. [14], scalar top pair production is analyzed in both a simplified model and phenomenologically tempered SUSY models in conserved R-parity using Run 1 data. The updated studies at $\sqrt{s} = 13$ TeV [15–18] have shown that a lighter stop mass region $m_{\tilde{t}_1} \lesssim 850$ GeV

is excluded at 95% C.L. when the lightest neutralino mass $m_{\tilde{\chi}_1^0}$ is less than about 300 GeV. On the other hand, $m_{\tilde{t}_1} \gtrsim 400\,\mathrm{GeV}$ and $m_{\tilde{\chi}_1^0} \gtrsim 300\,\mathrm{GeV}$ (with $m_{\tilde{t}_1} > m_{\tilde{\chi}_1^0}$) is still allowed. Another possibility is R-parity violation. Without R-parity, the lightest neutralino decays to the standard model particles, and thus the above analysis cannot be applied. In the R-parity-violated scenario, where especially $L_iL_jE_k^c$ or $L_iQ_jD_k^c$ types with light flavor indices exist, the stop mass below 1 TeV is excluded [19,20]. On the other hand, in $U_i^cD_j^cD_k^c$-type R-parity violation, a stop lighter than 1 TeV has not been excluded [21,22]. Thus, various possibilities have yet to be probed for the light stop scenario. The naturalness-inspired light stop scenario in the minimal supersymmetric standard model will be searched at the LHC with more data (see, e.g., Refs. [23–25] for recent studies). The electroweak precision test and future lepton collider may be other powerful options for the light stop search [26]. We show that high-energy longitudinal gauge boson scattering is another tool for the indirect search of the TeV-scale stop. We note that the present work focuses on the rather theoretical study of longitudinal W boson scattering. To discuss the discovery potential at collider experiments, one needs full simulation of the process, for example, $pp \to WWjj$, which is not covered in this paper. It is known that the observation of high-energy (over TeV) longitudinal gauge boson scattering would be challenging even in Run 2 at the LHC. We will discuss the issues in the last section, along with future prospects.

II. LIGHT SCALAR TOP SCENARIO

In this paper, we discuss two types of scenarios regarding the origin of the Higgs mass in the supersymmetric model:

(a) Higgs mass is explained in the MSSM particle contents.
(b) Other contributions besides the MSSM particles make the observed Higgs mass.

We assume that the other contributions to the Higgs mass are provided in a higher scale than stop mass, e.g., heavy vectorlike matters for scenario (b) (see, for example, Refs. [27–37]). To be concrete, we consider mass spectra $m_{\tilde{t}} \ll \tilde{m}$ for both cases. Here, $m_{\tilde{t}}$ and $\tilde{m}$ are the stop mass scale (defined later) and the mass scale of the rest of superparticles, respectively. It is similar to the so-called split supersymmetry model discussed in Ref. [38]. In split supersymmetry, gauginos are $\mathcal{O}$(1–10 TeV), and the other superparticles are much heavier. In the present discussion, we consider that stops (and the left-handed sbottom) are also around the TeV scale. Just to keep the grand unified theory (GUT) multiplet structure, we assume that the right-handed stau has TeV mass,[1] which does not affect the following analysis. Namely, our discussion comprises the SM-like Higgs with the scalar top, and it is independent of the details of the other sector. In Appendix, we also discuss the $m_{\tilde{t}} \sim \tilde{m}$ case for reference, which is also useful for an analytic check of the later calculation. In this paper, we do not argue the naturalness in the Higgs sector but focus on the consequence of a TeV-scale stop in the gauge boson scattering.

To define the relevant parameters for the Higgs mass, we give the MSSM superpotential along with soft SUSY breaking terms,

$$W_{\mathrm{MSSM}} = \lambda_t Q_3 \cdot H_u t_R^c + \mu_H H_u \cdot H_d + \cdots, \tag{1}$$

$$\mathcal{L}_{\mathrm{soft}} = A_t \lambda_t \tilde{Q}_3 \cdot H_u \tilde{t}_R^* - m_L^2 |\tilde{Q}_3|^2 - m_R^2 |\tilde{t}_R|^2 + \cdots, \tag{2}$$

where $Q_3 = (t_L, b_L)^T$, t_R^c, $H_u = (H_u^+, H_u^0)^T$, and $H_d = (H_d^0, H_d^-)^T$ are chiral superfields of the third-generation left-handed quark doublet, right-handed quark singlet (tilded fields are their superpartners), up-type Higgs doublet, and down-type Higgs doublet, respectively, and $A \cdot B \equiv A^T \epsilon B$ ($\epsilon = i\sigma_2$). An ellipsis indicates irrelevant terms in our following discussion. We assume that all parameters are real for simplicity. In the supersymmetric model, the stop loop contribution has a significant impact on the SM Higgs mass. In our study, we adopt the renormalization group (RG) method to determine the Higgs mass [8]. In the reference, the matching conditions at the scale $\mu \simeq \mu_{\tilde{t}} \sim m_{\tilde{t}}$ are given by

$$\lambda_{\mathrm{H}}^{\mathrm{SM}}(\mu_{\tilde{t}}) = \lambda_{\mathrm{H}}^{\mathrm{SM}'}(\mu_{\tilde{t}}) + \frac{N_C (y_t^{\mathrm{SM}'}(\mu_{\tilde{t}}))^4}{(4\pi)^2} \left[-\log\left(\frac{\mu_{\tilde{t}}^2}{m_{\tilde{t}}^2}\right) + \frac{X_t^2}{m_{\tilde{t}}^2}\left(1 - \frac{X_t^2}{12 m_{\tilde{t}}^2}\right)\right], \tag{3}$$

$$y_t^{\mathrm{SM}}(\mu_{\tilde{t}}) = y_t^{\mathrm{SM}'}(\mu_{\tilde{t}}), \tag{4}$$

where $\lambda_{\mathrm{H}}^{\mathrm{SM}}$ (y_t^{SM}) and $\lambda_{\mathrm{H}}^{\mathrm{SM}'}$ ($y_t^{\mathrm{SM}'}$) are the Higgs quartic coupling (top Yukawa coupling) in the energy regions $\mu < m_{\tilde{t}}$ and $m_{\tilde{t}} \le \mu (< \tilde{m})$, respectively. $N_C = 3$, $m_{\tilde{t}} = \sqrt{m_{\tilde{t}_1} m_{\tilde{t}_2}}$ ($m_{\tilde{t}_1}$, $m_{\tilde{t}_2}$ are stop masses), and $X_t = A_t + \mu_H \cot\beta$ ($\tan\beta = \langle H_u^0 \rangle / \langle H_d^0 \rangle$). $\lambda_{\mathrm{H}}^{\mathrm{SM}}$ must coincide with the Higgs quartic coupling in the SM. In Eq. (3), the second term on the right-hand side is the threshold correction by integrating out stops. In the numerical analysis, we solve RG equations for the gauge coupling constants, top Yukawa coupling, and Higgs quartic coupling. [In the numerical study, we will use more accurate expression for the condition (3). See the later discussion.] For scenario (a), we need to determine X_t for a given $m_{L,R}$ to obtain the observed Higgs mass. Thus, we solve the RG equations in the region $m_t \le \mu$ where m_t is the top mass. We refer to Refs. [39,40] for $m_t \le \mu \le \mu_{\tilde{t}}$ and

[1]For example, gauge coupling unification is kept at the level of 0.7–1% for $\tilde{m} = 10^{6\text{–}12}$ GeV and $m_{\tilde{t}} = 1$ TeV in one-loop calculation.

$\mu_{\tilde{t}} \le \mu \le \mu_{\rm SUSY}(\sim\tilde{m})$, respectively. The RG equations for $\mu_{\rm SUSY} \le \mu$ are well known, e.g., see Ref. [41]. Here, matching conditions at $\mu \simeq \mu_{\rm SUSY}$, $\lambda_{\rm H}^{\rm SM'}(\mu_{\rm SUSY}) = \frac{1}{8} g_Z^2(\mu_{\rm SUSY})\cos^2 2\beta$, and $y_t^{\rm SM'}(\mu_{\rm SUSY}) = \lambda_t(\mu_{\rm SUSY})\sin\beta$ [$g_Z^2 = g'^2 + g^2$ where g' and g are the gauge coupling constants of $U(1)_Y$ and $SU(2)_L$, respectively] should be used. (The solutions in this region are unnecessary for the computation of the scattering amplitudes. We use them for a check of the GUT unification.) We have checked that the obtained Higgs mass is consistent with the results by using the FeynHiggs package [42]; i.e., it agrees within about 2 (6) GeV in the $X_t < 0$ (>0) region. This accuracy suffices for leading-order analysis of longitudinal gauge boson scattering discussed below. On the other hand, for scenario (b), assuming an additional contribution to the Higgs quartic coupling at high energy, such as by vectorlike matters, we only need to solve the RG equations in $\mu \le \mu_{\tilde{t}}$ in the SM particle contents. In the later analysis, we will take $\mu_{\tilde{t}} = m_{\tilde{t}}$ and $\mu_{\rm SUSY} = \tilde{m}$.

Note that Eq. (3) corresponds to leading-order computation in the order counting method shown in Ref. [13]. In the literature, an auxiliary expansion parameter ξ is introduced to define the leading-order term for each physical quantity. Following their analysis, we assign

$$\lambda_{\rm H}^{\rm SM,SM'} \to \xi^2 \lambda_{\rm H}^{\rm SM,SM'}, \qquad y_t^{\rm SM,SM'} \to \xi^{1/2} y_t^{\rm SM,SM'}, \qquad g' \to \xi g', \qquad g \to \xi g. \tag{5}$$

In this assignment, any physical quantities, e.g., $\mathcal{P}$, can be given as $\mathcal{P} = \xi^n \sum_{i=0}^{\infty} p_i \xi^i$ in perturbative expansion. Then, we define p_0 as the leading order. Getting back to Eq. (3), both first and second terms in the right-hand side are counted as ξ^2, which means that not only the first term but also the second term is the leading order. Thus, we regard it as the leading-order matching condition. In Eq. (5), we have additionally assigned the ξ counting for g' and g for consistency, which is discussed later [see Eqs. (10) and (11)]. With this assignment, we have neglected terms such as $g^2\lambda_{\rm H}^{\rm SM}$ and g^4 in Eq. (3), which are ξ^4. In the following discussion, we use this method to compute the scattering amplitudes at the leading order.

Before performing the actual calculation, let us estimate the scattering amplitude. As pointed out in Ref. [13], the deviation from the SM in the amplitude high-energy gauge boson scattering is written in terms of the off-shell region of the Higgs propagator. Although the model is different, scalar tops are expected to play a role similar to that of the singlet scalars in the reference. Then, the deviation from the SM at the leading-order calculation is roughly estimated as

$$\Delta\mathcal{A} \sim \frac{N_c y_t^4}{(4\pi)^2}\left[\log\left(\frac{p^2}{m_{\tilde{t}}^2}\right) + \mathcal{O}\left(\frac{X_t^2}{p^2}\right)\right], \tag{6}$$

for $|p^2| \gg m_Z^2$ (m_Z is the Z boson mass), where $y_t \sim y_t^{\rm SM} \sim y_t^{\rm SM'}$, and p is the typical momentum of the scattering process. The logarithmic term, which is from divergent stop loop diagrams, is the dominant part for $|p^2| \gg m_{\tilde{t}}^2, X_t^2$, and it can be understood in terms of the RG flow of the Higgs quartic coupling. However, as emphasized in Ref. [13], detailed kinematics, such as energy dependence or angular distribution, of the scattering process cannot be described merely in RG computation. In addition, the second term of the bracket, which cannot be taken into account by RG computation, may also be comparable to the logarithmic term when $|p^2| \sim m_{\tilde{t}}^2, X_t^2$. Our main goal is to quantitatively show the behavior of the gauge boson scattering amplitudes in the existence of scalar tops in the SUSY model.

III. NAMBU-GOLDSTONE BOSON SCATTERING

A. Equivalence theorem

Since we are interested in high-energy longitudinal gauge boson scattering, the equivalence theorem can be applied in our calculation. The equivalence theorem tells us that the high-energy longitudinal gauge boson ($W_L^{\pm}, Z_L$) corresponds to Nambu-Goldstone (NG) boson ($G^{\pm}$, G^0). First, we will check the validity of the equivalence theorem quantitatively. To this end, we compare the differential cross section in center-of-mass frame for the processes $W_L^+W_L^{\pm} \to W_L^+W_L^{\pm}$ and $G^+G^{\pm} \to G^+G^{\pm}$ in the SM. The results are summarized in Table I. Here, we use the tree-level analytic formulas given in Ref. [13] and take the same input parameters, i.e., $m_W = 80.385$ GeV (W boson mass), $m_Z = 91.1876$ GeV, $m_h = 125.03$ GeV [43,44], and $g = 0.65178$. θ is the scattering angle. The deviations between G^+G^+ and $W_L^+W_L^+$ ($\cos\theta = 0$) are 14%, 4.9%, 1.2%, 0.19%, and 0.047% for center-of-mass energy $\sqrt{s} = 0.6$ 1, 2, 5, and 10 TeV, respectively. On the other hand, for W^+W^- (G^+G^-) scattering, the deviations are 21%, 10%, 2.5%, 0.40%, and 0.10% in the same $\sqrt{s}$ but for $\cos\theta = 0.5$. It is seen that the deviation gets smaller for larger $\sqrt{s}$ as expected. In

TABLE I. Differential cross section for $W_L^+W_L^+ \to W_L^+W_L^+$ and $G^+G^+ \to G^+G^+$ (upper) and $W_L^+W_L^+ \to W_L^+W_L^+$ and $G^+G^- \to G^+G^-$ (lower).

$W_L^+W_L^+$ vs. G^+G^+ ($\cos\theta = 0$)					
$\sqrt{s}$ [TeV]	0.6	1	2	5	10
$[d\sigma/d\cos\theta]_{G^+G^+}$ [pb]	9.571	3.446	0.8614	0.1378	0.03446
$[d\sigma/d\cos\theta]_{W_L^+W_L^+}$ [pb]	8.361	3.286	0.8513	0.1376	0.03444

$W_L^+W_L^-$ vs. G^+G^- ($\cos\theta = 0.5$)					
$\sqrt{s}$ [TeV]	0.6	1	2	5	10
$[d\sigma/d\cos\theta]_{G^+G^-}$ [pb]	1.509	0.5431	0.1358	0.02173	0.005431
$[d\sigma/d\cos\theta]_{W_L^+W_L^-}$ [pb]	1.913	0.5974	0.1392	0.02181	0.005437

the backward region, on the other hand, the differential cross section is suppressed due to a cancellation in the tree-level amplitude. In such a region, the other one-loop contributions besides (scalar) top and bottom, i.e., electroweak corrections, including the Sudakov logarithm [45,46], become numerically important [47]. It is discussed in Ref. [47] that the finite decay width of W bosons must be taken into account by using the complex mass scheme [48] or considering the actual decay chains of W bosons [49] for consistent calculation. Since those issues are beyond the scope of the present study, we discard backward region.[2]

In the later numerical analysis, we discuss the differential cross section in the SM and the supersymmetric model at the level of $\mathcal{O}(1$–$10\%)$. Thus, to substitute the NG boson scattering for longitudinal W boson scattering at less than about 0.1%, we will mainly consider $\sqrt{s} \geq 2$ TeV. Note that the number of events where the W boson system has the invariant mass over 2 TeV is expected to be limited even in Run 2 at the LHC. As mentioned in the Introduction, we try to show a potential of WW scattering for the study of beyond the SM in a long-term period, considering in the future a high-energy frontier experiment, such as the Future Circular Collider.

B. Scattering amplitudes

In this subsection, we will calculate the $G^+G^\pm \to G^+G^\pm$ scattering amplitude. The interaction terms which are relevant for the scattering processes in our current setup are

$$\begin{aligned}\mathcal{L} = &-\lambda_{\rm H}^{\rm SM'}|G^+G^-|^2 - y_t^{\rm SM'} X_t(\tilde{b}_L^* \tilde{t}_R G^- + \tilde{b}_L \tilde{t}_R^* G^+) \\ &- \left[(y_t^{\rm SM'})^2 - \frac{1}{2} g_Z^2 \left(-\frac{1}{2} + \frac{2}{3}\sin^2\theta_W\right)\cos 2\beta\right]|\tilde{b}_L|^2|G^+|^2 \\ &- \left[(y_t^{\rm SM'})^2 + \frac{1}{2} g_Z^2 \frac{2}{3}\sin^2\theta_W \cos 2\beta\right]|\tilde{t}_R|^2|G^+|^2, \end{aligned} \tag{7}$$

where the couplings are defined in Eqs. (3) and (4) and θ_W is the Weinberg angle. In the following calculation, we take $\overline{\rm MS}$ scheme in dimensional regularization and use LoopTools [50] for the numerical study.

Let us discuss $G^+G^+ \to G^+G^+$ scattering first. The scattering amplitudes in the supersymmetric model and the SM are given by the form

$$\mathcal{A}_{G^+G^+} = \mathcal{A}^{\rm tree}_{G^+G^+} + \mathcal{A}^{t\text{-}b}_{G^+G^+} + \mathcal{A}^{\tilde{t}\text{-}\tilde{b}}_{G^+G^+}, \tag{8}$$

$$\mathcal{A}^{\rm SM}_{G^+G^+} = \mathcal{A}^{\rm SM,tree}_{G^+G^+} + \mathcal{A}^{{\rm SM},t\text{-}b}_{G^+G^+}, \tag{9}$$

where "tree," "t-b," and "$\tilde{t}$-$\tilde{b}$" indicate the tree-level amplitude, top-bottom loop amplitude, and stop-sbottom loop amplitude, respectively, which are given by

$$\mathcal{A}^{\rm tree}_{G^+G^+} = -4\lambda_{\rm H}^{\rm SM'} - \frac{g_Z^2}{2}\left[\frac{t}{u} + \frac{u}{t} + 1\right], \tag{10}$$

$$\mathcal{A}^{\rm SM,tree}_{G^+G^+} = -4\lambda_{\rm H}^{\rm SM} - \frac{g_Z^2}{2}\left[\frac{t}{u} + \frac{u}{t} + 1\right], \tag{11}$$

$$\mathcal{A}^{t\text{-}b}_{G^+G^+} = -\frac{2N_c (y_t^{\rm SM'})^4}{(4\pi)^2}[B_0(t, m_t^2, m_t^2) + B_0(u, m_t^2, m_t^2)], \tag{12}$$

$$\mathcal{A}^{{\rm SM},t\text{-}b}_{G^+G^+} = -\frac{2N_c (y_t^{\rm SM})^4}{(4\pi)^2}[B_0(t, m_t^2, m_t^2) + B_0(u, m_t^2, m_t^2)], \tag{13}$$

where $t = (p_1 - k_1)^2$, $u = (p_1 - k_2)^2$ [p_i and k_i $(i, j = 1, 2)$ are momenta of incident and scattered particles, respectively], and B_0 is the loop function defined in Eq. (B.5) in Ref. [13] without $1/\bar{\epsilon}$. The couplings are renormalized ones, and their μ dependence is implicit. Here, we have taken the leading terms in the $|t|, |u| \gg m_Z^2$ limit. $\mathcal{A}^{\tilde{t}\text{-}\tilde{b}}_{G^+G^+}$ consists of three types of diagrams, circle, triangle, and box types, which are shown in Fig. 1. We can derive them straightforwardly as

$$\mathcal{A}^{\tilde{t}\text{-}\tilde{b}}_{G^+G^+} = \mathcal{A}^{\tilde{t}\text{-}\tilde{b},{\rm cir}}_{G^+G^+} + \mathcal{A}^{\tilde{t}\text{-}\tilde{b},{\rm tri}}_{G^+G^+} + \mathcal{A}^{\tilde{t}\text{-}\tilde{b},{\rm box}}_{G^+G^+}, \tag{14}$$

with

$$\mathcal{A}^{\tilde{t}\text{-}\tilde{b},{\rm cir}}_{G^+G^+} = \frac{N_C (y_t^{\rm SM'})^4}{(4\pi)^2}[s_{\theta_t}^4 B_0(t, m_{\tilde{t}_1}^2, m_{\tilde{t}_1}^2) + c_{\theta_t}^4 B_0(t, m_{\tilde{t}_2}^2, m_{\tilde{t}_2}^2) + 2s_{\theta_t}^2 c_{\theta_t}^2 B_0(t, m_{\tilde{t}_1}^2, m_{\tilde{t}_2}^2) + B_0(t, m_{\tilde{b}_L}^2, m_{\tilde{b}_L}^2)] + (t \to u\,\text{term}), \tag{15}$$

$$\begin{aligned}\mathcal{A}^{\tilde{t}\text{-}\tilde{b},{\rm tri}}_{G^+G^+} = &\frac{2N_C (y_t^{\rm SM'})^4 X_t^2}{(4\pi)^2}[s_{\theta_t}^4 C_0(0, t, 0, m_{\tilde{b}_L}^2, m_{\tilde{t}_1}^2, m_{\tilde{t}_1}^2) + c_{\theta_t}^4 C_0(0, t, 0, m_{\tilde{b}_L}^2, m_{\tilde{t}_2}^2, m_{\tilde{t}_2}^2) + 2s_{\theta_t}^2 c_{\theta_t}^2 C_0(0, t, 0, m_{\tilde{b}_L}^2, m_{\tilde{t}_1}^2, m_{\tilde{t}_2}^2) \\ &+ s_{\theta_t}^2 C_0(0, t, 0, m_{\tilde{t}_1}^2, m_{\tilde{b}_L}^2, m_{\tilde{b}_L}^2) + c_{\theta_t}^2 C_0(0, t, 0, m_{\tilde{t}_2}^2, m_{\tilde{b}_L}^2, m_{\tilde{b}_L}^2)] + (t \to u\ \text{term}), \end{aligned} \tag{16}$$

[2]Here, note that we do not insist that the forward region is effective for our study. As we will see later, it is dominated by γ and Z boson exchange diagrams and not so efficient for seeing the deviation from the SM. (Central or semicentral regions are more promising.)

$$\mathcal{A}^{\tilde{t}\text{-}\tilde{b},\mathrm{box}}_{G^+G^+} = \frac{2N_C(y_t^{\mathrm{SM}'})^4X_t^4}{(4\pi)^2}[s_{\theta_t}^4 D_0(0,0,0,0,u,t,m^2_{\tilde{b}_L},m^2_{\tilde{t}_1},m^2_{\tilde{b}_L},m^2_{\tilde{t}_1}) + c_{\theta_t}^4 D_0(0,0,0,0,u,t,m^2_{\tilde{b}_L},m^2_{\tilde{t}_2},m^2_{\tilde{b}_L},m^2_{\tilde{t}_2}) + 2s^2_{\theta_t}c^2_{\theta_t}D_0(0,0,0,0,u,t,m^2_{\tilde{b}_L},m^2_{\tilde{t}_1},m^2_{\tilde{b}_L},m^2_{\tilde{t}_2})]. \tag{17}$$

Loop functions C_0 and D_0 are those defined in Ref. [50]. $m_{\tilde{b}_L}$ is the left-handed sbottom mass. Since we consider that the right-handed sbottom mass is much larger than the third-generation left-handed squark mass, the lighter sbottom is mostly composed of b_L; thus, $m_{\tilde{b}_L} \simeq m_L$. θ_t is the mixing angle in stop sector defined as $(\tilde{t}_1,\tilde{t}_2)^T = Z(\tilde{t}_L,\tilde{t}_R)^T$ with orthogonal matrix $Z_{11} = \cos\theta_t \equiv c_{\theta_t}$, $Z_{12} = \sin\theta_t \equiv s_{\theta_t}$. To be consistent with ξ expansion analysis, we have omitted terms such as $(y_t^{\mathrm{SM}'})^2 g_Z^2$ and g_Z^4 in Eq. (15), which

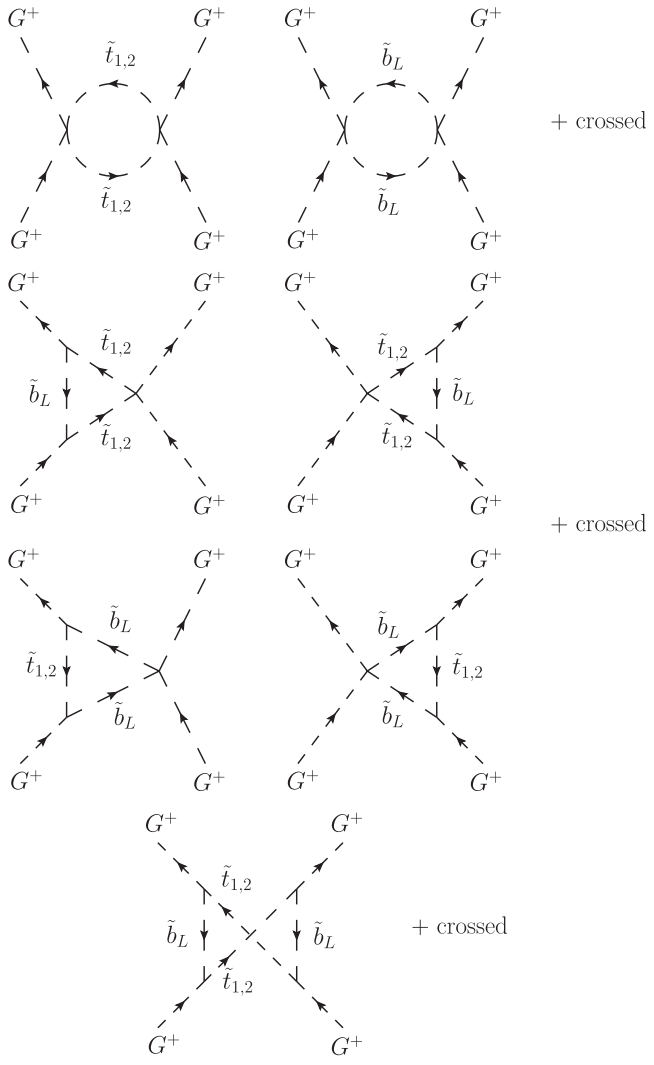

FIG. 1. Stop-sbottom loop diagrams which induce G^+G^+ scattering. Time flows upward, and "crossed" means crossed diagram for final-state bosons. Circle-type, triangle-type, and crossed box-type diagrams correspond to $\mathcal{A}^{\tilde{t}\text{-}\tilde{b},\mathrm{cir}}_{G^+G^+}$, $\mathcal{A}^{\tilde{t}\text{-}\tilde{b},\mathrm{tri}}_{G^+G^+}$, $\mathcal{A}^{\tilde{t}\text{-}\tilde{b},\mathrm{box}}_{G^+G^+}$ in Eq. (14), respectively.

are $\mathcal{O}(\xi^3)$ and $\mathcal{O}(\xi^4)$, respectively, in ξ expansion. We note that the explicit μ dependence coming from the B_0 function is canceled at the leading order by the RG flow of $\lambda_{\mathrm{H}}^{\mathrm{SM}}$ ($\lambda_{\mathrm{H}}^{\mathrm{SM}'}$). Since our goal is to compute the deviation at leading order in ξ expansion, we take $\mu = m_{\tilde{t}}$ in the amplitude hereafter.

Another scattering amplitude for the process $G^+G^- \to G^+G^-$ can be obtained by replacing the Mandelstam variable u by s.

Before going to the numerical analysis, let us check low-energy and high-energy limits. In the low-energy limit, the amplitudes $\mathcal{A}_{G^+G^+}$ and $\mathcal{A}_{G^+G^-}$ should coincide with those in the SM. To see this, we define $\Delta\mathcal{A}_{G^+G^\pm}$:

$$\Delta\mathcal{A}_{G^+G^\pm} = \mathcal{A}_{G^+G^\pm} - \mathcal{A}^{\mathrm{SM}}_{G^+G^\pm}. \tag{18}$$

Then, using the matching conditions (3) and (4), they are simply given by

$$\Delta\mathcal{A}_{G^+G^\pm} = \mathcal{A}^{\tilde{t}\text{-}\tilde{b}}_{G^+G^\pm} + \frac{4N_C(y_t^{\mathrm{SM}}(m_{\tilde{t}}))^4}{(4\pi)^2}\frac{X_t^2}{m_{\tilde{t}}^2}\left(1-\frac{X_t^2}{12m_{\tilde{t}}^2}\right). \tag{19}$$

In the low-energy limit, $s,|t|,|u| \ll m_{\tilde{t}}^2$ (but $s,|t|,|u| \gg m_Z^2$), and taking $m_{\tilde{t}_1} \simeq m_{\tilde{t}_2} \simeq m_L \simeq m_{\tilde{t}}$, the stop-sbottom loop contribution behaves as

$$\mathcal{A}^{\tilde{t}\text{-}\tilde{b},\mathrm{cir}}_{G^+G^\pm} \to \frac{4N_C(y_t^{\mathrm{SM}'}(\mu))^4}{(4\pi)^2}\log\left(\frac{\mu^2}{m_{\tilde{t}}^2}\right)\Bigg|_{\mu=m_{\tilde{t}}}, \tag{20}$$

$$\mathcal{A}^{\tilde{t}\text{-}\tilde{b},\mathrm{tri}}_{G^+G^\pm} \to \frac{8N_C(y_t^{\mathrm{SM}'}(\mu))^4X_t^2}{(4\pi)^2}\left(-\frac{1}{2m_{\tilde{t}}^2}\right)\Bigg|_{\mu=m_{\tilde{t}}}, \tag{21}$$

$$\mathcal{A}^{\tilde{t}\text{-}\tilde{b},\mathrm{box}}_{G^+G^\pm} \to \frac{2N_C(y_t^{\mathrm{SM}'}(\mu))^4X_t^4}{(4\pi)^2}\left(\frac{1}{6m_{\tilde{t}}^4}\right)\Bigg|_{\mu=m_{\tilde{t}}}, \tag{22}$$

which leads to

$$\mathcal{A}^{\tilde{t}\text{-}\tilde{b}}_{G^+G^\pm} \to -\frac{4N_C(y_t^{\mathrm{SM}}(m_{\tilde{t}}))^4}{(4\pi)^2}\left[\frac{X_t^2}{m_{\tilde{t}}^2}\left(1-\frac{X_t^2}{12m_{\tilde{t}}^2}\right)\right]. \tag{23}$$

Thus, $\Delta\mathcal{A}_{G^+G^-} \to 0$, which means that the amplitude asymptotically approaches the SM one in the low-energy limit as expected.

In numerical calculation, $m_{\tilde{t}_1} \simeq m_{\tilde{t}_2} \simeq m_{\tilde{t}}$ is not always satisfied. Therefore, in the later analysis, we use the following expressions instead of Eqs. (19) and (3):

$$\Delta\mathcal{A}_{G^+G^\pm} = \mathcal{A}^{\tilde{t}\text{-}\tilde{b}}_{G^+G^\pm} - \mathcal{A}^{\tilde{t}\text{-}\tilde{b}}_{G^+G^\pm}|_{s\to 0}, \tag{24}$$

$$\lambda_{\rm H}^{\rm SM}(\mu_{\tilde{t}}) = \lambda_{\rm H}^{\rm SM'}(\mu_{\tilde{t}}) - \frac{1}{4}\mathcal{A}^{\tilde{t}\text{-}\tilde{b}}_{G^+G^\pm}|_{s\to 0}. \tag{25}$$

In the high-energy limit $s, |t|, |u| \gg m_{\tilde{t}}, |X_t|$, on the other hand,

$$\mathcal{A}^{\tilde{t}\text{-}\tilde{b}}_{G^+G^+} \to \frac{4N_C(y_t^{\rm SM'}(m_{\tilde{t}}))^4}{(4\pi)^2}\left[\log\left(\frac{m_{\tilde{t}}^2}{\sqrt{tu}}\right) - 2 + \frac{m_{\tilde{t}}^2}{t}\left(\log\frac{m_{\tilde{t}}^2}{-t} - 1\right) + \frac{m_{\tilde{t}}^2}{u}\left(\log\frac{m_{\tilde{t}}^2}{-u} - 1\right) + \frac{X_t^2}{2t}\log^2\left(\frac{m_{\tilde{t}}^2}{-t}\right) + \frac{X_t^2}{2u}\log^2\left(\frac{m_{\tilde{t}}^2}{-u}\right)\right] + \mathcal{O}\left(\frac{m_{\tilde{t}}^4, X_t^4}{|t|^2, |u|^2}\right), \tag{26}$$

$$\mathcal{A}^{\tilde{t}\text{-}\tilde{b}}_{G^+G^-} \to \frac{2N_C(y_t^{\rm SM'}(m_{\tilde{t}}))^4}{(4\pi)^2}\left[\log\left(\frac{m_{\tilde{t}}^2}{\sqrt{-st}}\right) - 2 + \frac{m_{\tilde{t}}^2}{s}\left(\log\frac{m_{\tilde{t}}^2}{s} - 1\right) + \frac{m_{\tilde{t}}^2}{t}\left(\log\frac{m_{\tilde{t}}^2}{-t} - 1\right) - \frac{i\pi}{2}\left(1 - 2\frac{m_{\tilde{t}}^2}{s}\right) + \frac{X_t^2}{2s}\left\{\log^2\left(\frac{m_{\tilde{t}}^2}{s}\right) - \pi^2 + 2i\pi\log\left(\frac{m_{\tilde{t}}^2}{s}\right)\right\} + \frac{X_t^2}{2t}\log^2\left(\frac{m_{\tilde{t}}^2}{-t}\right)\right] + \mathcal{O}\left(\frac{m_{\tilde{t}}^4, X_t^4}{s^2, |t|^2}\right). \tag{27}$$

The first line on the right-hand side comes from circle diagram, which agrees with the native estimation (6) and can be understood in terms of the RG flow of the Higgs quartic coupling. Meanwhile, the others are derived in the explicit calculation of Feynman diagrams, which cannot be described by the RG equations and are necessary ingredients for the numerical analysis of the scattering processes.

IV. NUMERICAL RESULTS

Now, we are ready to give the numerical result. To this end, we use the quantity

$$\Delta_{G^+G^\pm} = \frac{|\mathcal{A}_{G^+G^\pm}|^2 - |\mathcal{A}^{\rm SM}_{G^+G^\pm}|^2}{|\mathcal{A}^{\rm SM}_{G^+G^\pm}|^2}, \tag{28}$$

which corresponds to the deviation from the SM for the differential cross section.

Figure 2 shows the result for the G^+G^+ process as a function of $\sqrt{s}$ for the fixed scattering angle, $\cos\theta = 0$. We take $m_L = m_R = 0.5$, 1, and 2 TeV (left) and $m_L = 2m_R = 1$ and 2 TeV (right) with $X_t = 0.5m_L$ at $\mu = m_{\tilde{t}}$, which corresponds to scenario (b) discussed in Sec. II. Roughly speaking, the left (right) panel covers the situation of the degenerate (split) mass spectrum in the stop sector.

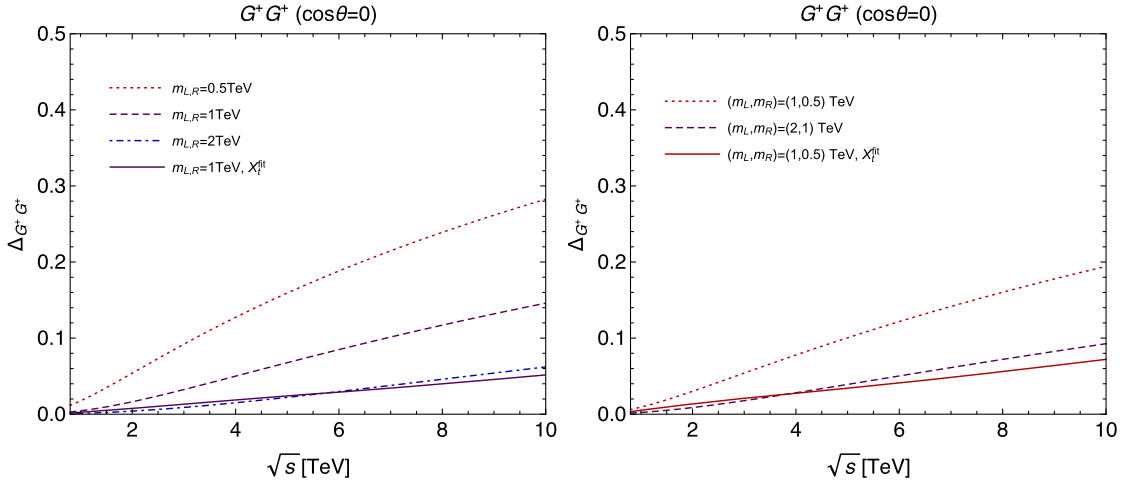

FIG. 2. Deviation from the SM for the G^+G^+ scattering process, defined in Eq. (28), as a function of center-of- mass energy $\sqrt{s}$. The scattering angles are taken as $\cos\theta = 0$. (Left) $m_L = m_R = 0.5$ (red dotted), 1 (purple dashed), and 2 (blue dot-dashed) TeV with $X_t = 0.5m_L$ at $\mu = m_{\tilde{t}}$. In $X_t^{\rm fit}$ (purple solid) line, $X_t = 1.82$ TeV, which gives the observed Higgs mass for $m_L = m_R = 1$ TeV, is taken. (Right) $m_L = 2m_R = 1$ (red dotted) and 2 (purple dashed) TeV with $X_t = 0.5m_L$ at $\mu = m_{\tilde{t}}$. In $X_t^{\rm fit}$ (red solid) line, $X_t = 1.45$ TeV, which gives the observed Higgs mass, is taken.

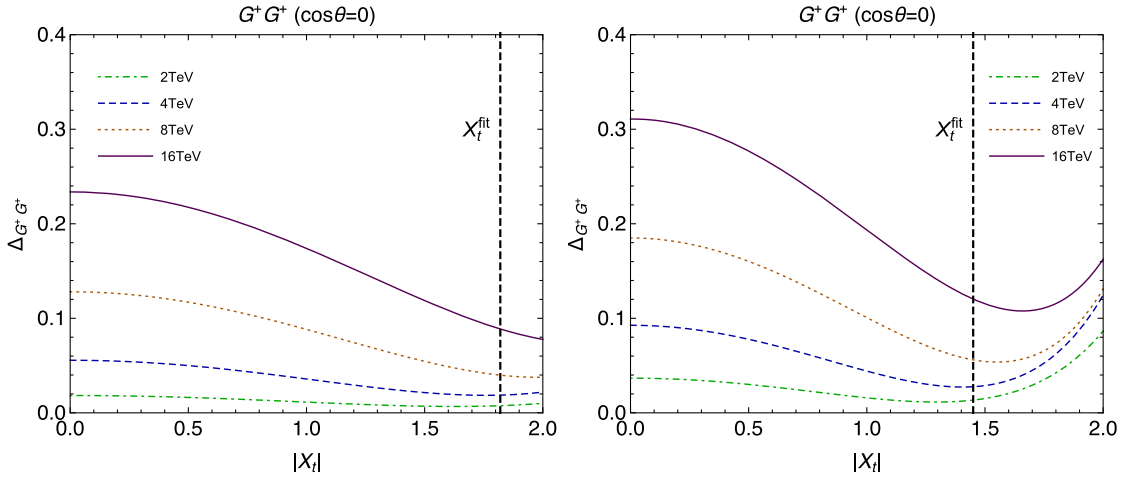

FIG. 3. X_t and $\sqrt{s}$ dependence of the amplitude for G^+G^+ process. $m_L = m_R = 1$ TeV (left) and $m_L = 2m_R = 1$ TeV (right) are taken. Line contents are $\sqrt{s} = 2$ (green dot-dashed), 4 (blue dashed), 8 (orange dotted), and 16 TeV (purple solid). Locations of $X_t^{\rm fit}$ are also indicated.

For scenario (a), the results for $m_L = m_R = 1$ TeV with $X_t = X_t^{\rm fit} = 1.82$ TeV (left) and $m_L = 2m_R = 1$ TeV with $X_t = X_t^{\rm fit} = 1.45$ TeV (right) are given. Here, we omit another larger value of $|X_t|$ to give the observed Higgs mass since it would not be phenomenologically acceptable due to the vacuum instability bound $X_t/\sqrt{m_{\tilde{t}_1}^2 + m_{\tilde{t}_2}^2} \lesssim \sqrt{3}$ [51] (see also the earlier analysis to give the bound $X_t/\sqrt{m_{\tilde{t}_1}^2 + m_{\tilde{t}_2}^2} \lesssim \sqrt{7}$ [52].)[3]

It is seen that the deviation increases monotonically as $\sqrt{s}$ gets large for fixed $m_{L,R}$ and X_t. It is attributed to the logarithmic term [first term of Eq. (26)], which originates in the stop-sbottom loop and can be understood by RG running of the Higgs quartic coupling.[4] A smaller $m_{L,R}$ gives a larger deviation. For example, $\Delta_{G^+G^+} = 16$ (28)%, 7 (15)%, and 2 (6)% for $\sqrt{s} = 5$ (10) TeV for $m_{L,R} = 0.5$, 1, and 2 TeV with $X_t = 0.5m_L$, respectively. This is because the $\log(m_{\tilde{t}}^2/\sqrt{tu})$ term, which is dominant in $\mathcal{A}_{G^+G^+}^{\tilde{t}-\tilde{b}}$ [see Eq. (26)], contributes constructively in the total amplitude for $\sqrt{s} > m_{\tilde{t}}$. It is true for the split mass spectrum (right panel).

When $X_t = X_t^{\rm fit}$, on the other hand, $\Delta_{G^+G^+}$ gets smaller compared to the result with the same $m_{L,R}$ but $X_t = 0.5m_L$. To understand the behavior, we plot $\Delta_{G^+G^+}$ as a function of X_t for various $\sqrt{s}$ in Fig. 3 for $m_L = m_R = 1$ TeV (left) and $m_L = 2m_R = 1$ TeV (right). It is found that $\Delta_{G^+G^+}$ decreases as X_t increases for $X_t \lesssim X_t^{\rm fit}$, which can be understood from Eqs. (24) [or (19)] and (26). The second term on the right-hand side of Eq. (24) is positive and destructively interferes with $\mathcal{A}_{G^+G^+}^{\tilde{t}-\tilde{b}}$ for $X_t \lesssim X_t^{\rm fit}(\sim m_{\tilde{t}})$.

For larger $|\cos\theta|$, the deviation gets smaller since Z and γ exchange terms which are proportional to $1/u$ or $1/t$ dominate the scattering amplitude. For example, when $\cos\theta = 0.5$, $\Delta_{G^+G^+} = 11(18)\%$, 4.8(10)%, and 2(4)% for $\sqrt{s} = 5(10)$ TeV $m_L = m_R = 0.5$, 1, and 2 TeV with $X_t = 0.5m_L$, respectively.

G^+G^- scattering has similar behavior except for a bump, which corresponds to a resonance at $\sqrt{s} \simeq 2m_{\tilde{t}}$ in Fig. 4. This bump is due to the discontinuity of the first derivative of $B_0(q^2, m_1^2, m_2^2)$ with respect to q^2 at $q^2 \simeq (m_1 + m_2)^2$. For $\sqrt{s} \lesssim 2m_{\tilde{t}}$, the stop-sbottom loop (dominated by circle diagrams) is positive, which constructively interferes with tree plus top-bottom loop contributions. In the region $\sqrt{s} \gtrsim 2m_{\tilde{t}}$, on the other hand, $\Delta_{G^+G^-}$ monotonically decreases. This is because the dominant term $\log(m_{\tilde{t}}^2/\sqrt{-st})$ in Eq. (27) is negative, which is destructive in the total amplitude at the high-energy range. For example, $\Delta_{G^+G^-} = -29$ $(-42)\%$, -11 $(-25)\%$, and 6 $(-9)\%$ for $\sqrt{s} = 5(10)$ TeV, and $\cos\theta = 0.5$ for $m_L = m_R = 0.5$, 1, and 2 TeV with $X_t = 0.5m_L$, respectively (left panel). Qualitatively, the same behavior is seen for the split mass case (right panel). Regarding X_t dependence, it is seen that $|\Delta_{G^+G^-}|$ gets smaller for $X_t = X_t^{\rm fit}$ similarly to the G^+G^+ case. Figure 5 clarifies the behavior. It is found that $|\Delta_{G^+G^-}|$ decreases in the $X_t \lesssim m_{\tilde{t}}$ region, which is attributed to the second term on the right-hand side of Eq. (24) as explained in the G^+G^+ case.

Thus, in both the G^+G^+ and G^+G^- scattering processes, it would be difficult to observe the deviation from the SM in

[3]We have checked that in this region of X_t the ρ parameter is within the 2σ bound of the observed value $\Delta\rho = (4.2 \pm 2.7) \times 10^{-4}$ [53] based on Refs. [23,54–56]. It is also confirmed that Higgs-gluon-gluon coupling is within 25% [57] of the SM value referring to Refs. [58,59].

[4]The calculation is valid in a much higher $\sqrt{s}$ value, and a larger deviation is given in the energy range. However, it might be unnecessary information for a realistic (future) collider search; thus, we have omitted it.

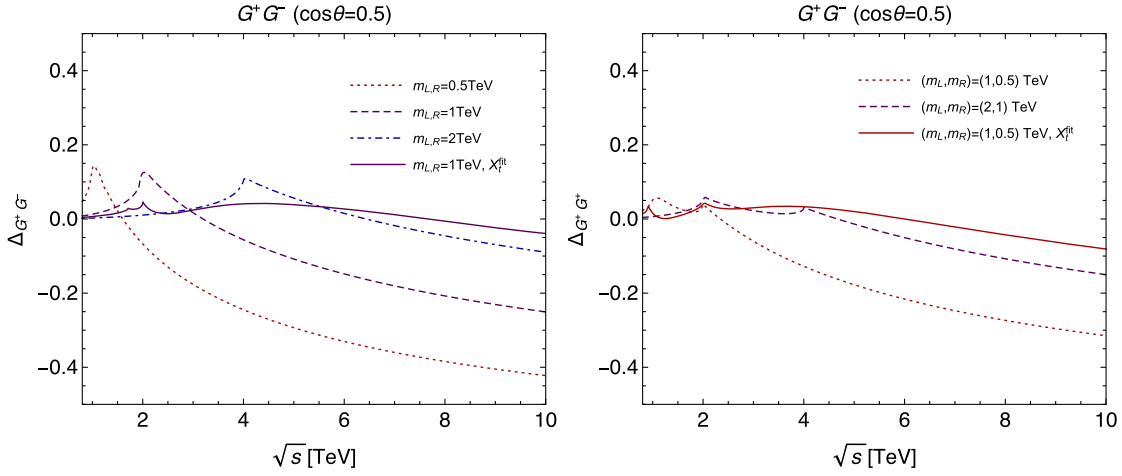

FIG. 4. Same as Fig. 2 but for the G^+G^- scattering process taking $\cos\theta = 0.5$.

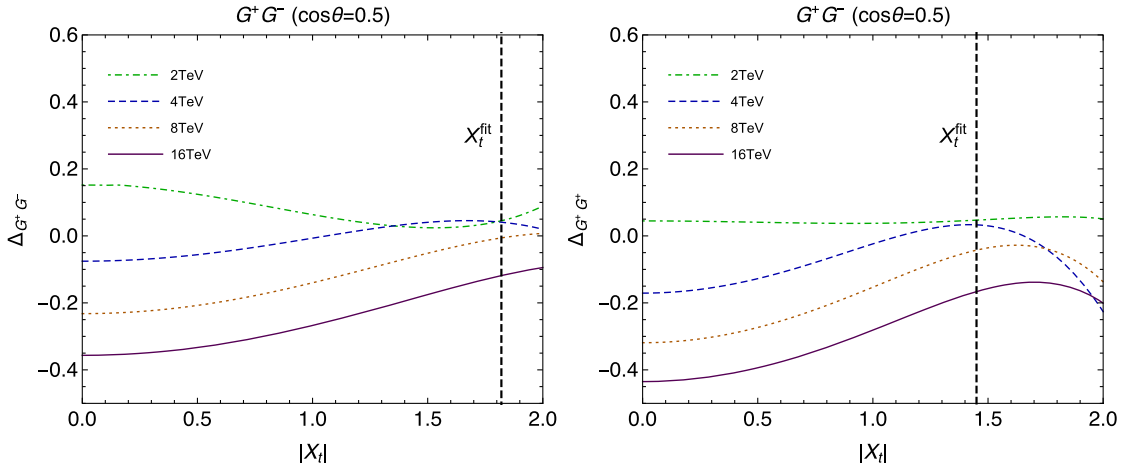

FIG. 5. Same as Fig. 3 but for the G^+G^- process taking $\cos\theta = 0.5$.

the parameter space $|X_t| \sim m_{\tilde{t}}$, especially $X_t \simeq X_t^{\rm fit}$, since $\Delta_{G^+G^\pm}$ is a few percent. In other words, scenario (a) is like a "blind spot" for the TeV-scale stop search in the longitudinal W boson scattering processes. In scenario (b), on the other hand, $\mathcal{O}(1$–$10\%)$ deviation is expected for $\sqrt{s} = 1$–10 TeV.

V. CONCLUDING REMARKS

In this paper, we have studied high-energy longitudinal W boson scattering with a light scalar top of which the mass is a few hundred GeV to a few TeV. They affect the SM Higgs potential at the quantum level, and consequently the deviation from the standard model in longitudinal gauge boson scattering is expected from the equivalence theorem. Applying the equivalence theorem, we have computed charged Nambu-Goldstone boson scattering processes and substituted them as high-energy $W_L^+W_L^\pm$ scattering processes. In the study, we consider two scenarios: (a) Higgs mass is explained in the MSSM particle contents, and (b) other contributions besides the MSSM particles make the observed Higgs mass. It has been found that $\mathcal{O}(1$–$10\%)$ deviation in the differential cross section is predicted depending on stop mass and kinematics. As an example of b, for $\sqrt{s} = 5$ (10) TeV and $\cos\theta = 0$, the deviation in the $W_L^+W_L^+$ process is 16 (28)% and 7 (15)% when both left- and right-handed stop masses (m_L and m_R) are 0.5 and 1 TeV with the mixing parameter $X_t = 0.5m_L$, respectively. Similarly, in $W_L^+W_L^-$, it is -29 (-42)% and -11 (-25)% but for $\cos\theta = 0.5$. For scenario (a), on the other hand, it has been discovered that the deviation gets smaller, e.g., 2 (4)% and 4 (-4)% for $m_L = m_R = 1$ TeV with the appropriate X_t for $\sqrt{s} = 5(10)$ in $W_L^+W_L^+$ and $W_L^+W_L^-$, respectively. The same behavior is seen for the $m_L \neq m_R$ case. Thus, in such a case, it would be challenging to see the existence of the stop in W_LW_L scattering.

High-energy longitudinal gauge boson scattering has started to be measured at the LHC [60,61]. However, the observation of $\mathcal{O}(10\%)$ deviation would be difficult even in Run 2 at the LHC. This is because the number of events which has over a few TeV invariant mass of the W boson system is suppressed due to gauge cancellation [62]. (We have checked this by using the MadGraph package [63].[5]) Thus, at least an upgraded program, such as the High Luminosity LHC, would be necessary. Or the Future Circular Collider, which is planed to operate at 100 TeV center-of-mass energy, would be more promising for the study of the gauge boson scattering. In such a high-energy experiment, the observation of stop or sbottom pair production might be a more direct and easier way to observe a clue of the supersymmetry. As mentioned in the Introduction, however, there are model dependence in the data analysis, e.g., details of the decay modes, or violation of R-parity. High-energy longitudinal gauge boson scattering would be complementary to the direct searches. We have provided the theoretical ingredients for the numerical study and discussed feasibility of the discovery of scalar tops in the longitudinal gauge boson scattering. The next step will be to perform a full simulation for hadron or lepton collider experiments with various energies, for which Refs. [47,49,64–73] are useful. We leave it to future work.

ACKNOWLEDGMENTS

We are grateful to Kazuhiro Endo and Yukinari Sumino for valuable discussions. This work was supported by MEXT KAKENHI Grant No. 17H05402 and JSPS KAKENHI Grant No. 17K14278 (K. I.).

APPENDIX: ANALYTIC CHECK

We will check that the G^+G^+ and G^+G^- scattering amplitudes reduce to those in the SM in low-energy limit by using the analytic Higgs mass formula for the $\tilde{m} \sim m_{\tilde{t}}$ case.

First of all, we need to use the Lagrangian after the following replacement:

$$\lambda_{\rm H}^{\rm SM'} \to \frac{1}{8} g_Z^2 \cos^2 2\beta, \qquad y_t^{\rm SM'} \to \lambda_t \sin\beta. \tag{A1}$$

Consequently, the matching conditions are

$$\lambda_{\rm H}^{\rm SM}(\mu_{\tilde{t}}) = \frac{1}{8} g_Z^2 \cos^2 2\beta(\mu_{\tilde{t}}) + \frac{N_C (y_t^{\rm SM'}(\mu_{\tilde{t}}))^4}{(4\pi)^2} \left[-\log\left(\frac{\mu_{\tilde{t}}^2}{m_{\tilde{t}}^2}\right) + \frac{X_t^2}{m_{\tilde{t}}^2}\left(1 - \frac{X_t^2}{12 m_{\tilde{t}}^2}\right)\right], \tag{A2}$$

$$y_t^{\rm SM}(\mu_{\tilde{t}}) = \lambda_t \sin\beta(\mu_{\tilde{t}}). \tag{A3}$$

In the MSSM where $\tilde{m} \sim m_{\tilde{t}}$, the SM Higgs mass is given by analytically using the effective potential [4–7][6]

$$(m_h^{\rm MSSM})^2 \simeq m_Z^2 \cos^2 2\beta + \frac{2N_c (\lambda_t \sin\beta)^4 v^2}{(4\pi)^2} \left[\log\left(\frac{m_{\tilde{t}}^2}{m_t^2}\right) + \frac{X_t^2}{m_{\tilde{t}}^2}\left(1 - \frac{X_t^2}{12 m_{\tilde{t}}^2}\right)\right]. \tag{A4}$$

Using this expression, it is found that the X_t dependence on $m_h^{\rm MSSM}$ and the one obtained by using the RG equation in the text agree within around 1 GeV when we take $\mu = m_{\tilde{t}}$ for top Yukawa coupling. Hereafter, we take $\mu = m_{\tilde{t}}$.

G^+G^+ and G^+G^- scattering amplitudes are easily obtained by using the previous result along with the above replacement and matching conditions. Now, let us see the low-energy limit, $s, |t|, |u| \ll m_{\tilde{t}}^2$ (but $s, |t|, |u| \gg m_Z^2$). $\mathcal{A}^{\tilde{t}-\tilde{b}}_{G^+G^\pm}$ corresponding to Eq. (23) is the same expression. Then, combining with

$$\mathcal{A}^{t\text{-}b}_{G^+G^+} \to -\frac{4N_c (y_t^{\rm SM})^4}{(4\pi)^2}\left[\log\left(\frac{\mu^2}{\sqrt{tu}}\right) + 2\right]\Big|_{\mu=m_{\tilde{t}}}, \tag{A5}$$

$$\mathcal{A}^{t\text{-}b}_{G^+G^-} \to -\frac{4N_c (y_t^{\rm SM})^4}{(4\pi)^2}\left[\log\left(\frac{\mu^2}{\sqrt{st}}\right) + 2\right]\Big|_{\mu=m_{\tilde{t}}}, \tag{A6}$$

and Eq. (A4), we obtain

$$\mathcal{A}_{G^+G^+} \to -\frac{2(m_h^{\rm MSSM})^2}{v^2} - \frac{g_Z^2}{2}\left[\frac{t}{u} + \frac{u}{t} + 1\right] - \frac{2N_c (y_t^{\rm SM})^4}{(4\pi)^2}\left[\log\left(\frac{m_t^4}{tu}\right) + 4\right], \tag{A7}$$

$$\mathcal{A}_{G^+G^-} \to -\frac{2(m_h^{\rm MSSM})^2}{v^2} - \frac{g_Z^2}{2}\left[\frac{s}{t} + \frac{t}{s} + 1\right] - \frac{2N_c (y_t^{\rm SM})^4}{(4\pi)^2}\left[\log\left(\frac{m_t^4}{st}\right) + 4\right]. \tag{A8}$$

This is exactly the amplitude including the top-bottom loop in the SM for $m_h^{\rm MSSM} = m_h$ [13].

[5]We thank Yasuhiro Shimizu for pointing this out and information useful for performing MadGraph5.

[6]For review, see Ref. [41]. For diagrammatic calculation, see, e.g., Ref. [9]. It is shown that the diagrammatic calculation agrees well with the result in the effective potential approach.

[1] G. Aad *et al.* (ATLAS Collaboration), Phys. Lett. B **716**, 1 (2012).
[2] S. Chatrchyan *et al.* (CMS Collaboration), Phys. Lett. B **716**, 30 (2012).
[3] ATLAS and CMS Collaborations, Report No. ATLAS-CONF-2015-044.
[4] H. E. Haber and R. Hempfling, Phys. Rev. Lett. **66**, 1815 (1991).
[5] J. R. Ellis, G. Ridolfi, and F. Zwirner, Phys. Lett. B **257**, 83 (1991).
[6] J. R. Ellis, G. Ridolfi, and F. Zwirner, Phys. Lett. B **262**, 477 (1991).
[7] Y. Okada, M. Yamaguchi, and T. Yanagida, Prog. Theor. Phys. **85**, 1 (1991).
[8] Y. Okada, M. Yamaguchi, and T. Yanagida, Phys. Lett. B **262**, 54 (1991).
[9] A. Brignole, Phys. Lett. B **281**, 284 (1992).
[10] D. Chway, T. H. Jung, H. D. Kim, and R. Dermisek, Phys. Rev. Lett. **113**, 051801 (2014).
[11] K. Endo and Y. Sumino, J. High Energy Phys. 05 (2015) 030.
[12] K. Hashino, S. Kanemura, and Y. Orikasa, Phys. Lett. B **752**, 217 (2016).
[13] K. Endo, K. Ishiwata, and Y. Sumino, Phys. Rev. D **94**, 075007 (2016).
[14] G. Aad *et al.* (ATLAS Collaboration), Eur. Phys. J. C **75**, 510 (2015); **76**, 153(E) (2016).
[15] ATLAS Collaboration, Report No. ATLAS-CONF-2016-07; Report No. ATLAS-CONF-2016-050; Report No. ATLAS-CONF-2016-076.
[16] M. Aaboud *et al.* (ATLAS Collaboration), Phys. Rev. D **94**, 032005 (2016).
[17] CMS Collaboration, Report No. CMS-PAS-SUS-16-014; Report No. CMS-PAS-SUS-16-015; Report No. CMS-PAS-SUS-16-028; Report No. CMS-PAS-SUS-16-029; Report No. CMS-PAS-SUS-16-030.
[18] V. Khachatryan *et al.* (CMS Collaboration), Eur. Phys. J. C **76**, 460 (2016).
[19] S. Chatrchyan *et al.* (CMS Collaboration), Phys. Rev. Lett. **111**, 221801 (2013).
[20] V. Khachatryan *et al.* (CMS Collaboration), Phys. Lett. B **760**, 178 (2016).
[21] G. Aad *et al.* (ATLAS Collaboration), J. High Energy Phys. 06 (2016) 067.
[22] ATLAS Collaboration, Report No. ATLAS-CONF-2016-022; Report No. ATLAS-CONF-2016-084.
[23] A. Pierce and B. Shakya, arXiv:1611.00771.
[24] H. Baer, V. Barger, N. Nagata, and M. Savoy, Phys. Rev. D **95**, 055012 (2017).
[25] M. Chala, A. Delgado, G. Nardini, and M. Quiros, J. High Energy Phys. 04 (2017) 097.
[26] J. Fan, M. Reece, and L. T. Wang, J. High Energy Phys. 08 (2015) 152.
[27] T. Moroi and Y. Okada, Mod. Phys. Lett. A **07**, 187 (1992).
[28] T. Moroi and Y. Okada, Phys. Lett. B **295**, 73 (1992).
[29] K. S. Babu, I. Gogoladze, and C. Kolda, arXiv:hep-ph/0410085.
[30] K. S. Babu, I. Gogoladze, M. U. Rehman, and Q. Shafi, Phys. Rev. D **78**, 055017 (2008).
[31] S. P. Martin, Phys. Rev. D **81**, 035004 (2010).
[32] M. Asano, T. Moroi, R. Sato, and T. T. Yanagida, Phys. Lett. B **705**, 337 (2011).
[33] M. Endo, K. Hamaguchi, S. Iwamoto, and N. Yokozaki, Phys. Rev. D **84**, 075017 (2011).
[34] J. L. Evans, M. Ibe, and T. T. Yanagida, arXiv:1108.3437.
[35] T. Moroi, R. Sato, and T. T. Yanagida, Phys. Lett. B **709**, 218 (2012).
[36] M. Endo, K. Hamaguchi, S. Iwamoto, and N. Yokozaki, Phys. Rev. D **85**, 095012 (2012).
[37] J. Hisano, W. Kuramoto, and T. Kuwahara, Prog. Theor. Exp. Phys. **2017**, 033B10 (2017).
[38] G. F. Giudice and A. Romanino, Nucl. Phys. **B699**, 65 (2004); Nucl. Phys. **B706**, 487(E) (2005).
[39] D. Buttazzo, G. Degrassi, P. P. Giardino, G. F. Giudice, F. Sala, A. Salvio, and A. Strumia, J. High Energy Phys. 12 (2013) 089.
[40] H. E. Haber and R. Hempfling, Phys. Rev. D **48**, 4280 (1993).
[41] M. Drees, R. Godbole, and P. Roy, *Theory and Phenomenology of Sparticles: An Account of Four-Dimensional N=1 Supersymmetry in High Energy Physics* (World Scientific, Singapore, 2004).
[42] S. Heinemeyer, W. Hollik, and G. Weiglein, Comput. Phys. Commun. **124**, 76 (2000); Eur. Phys. J. C **9**, 343 (1999).
[43] G. Aad *et al.* (ATLAS Collaboration), Phys. Rev. D **90**, 052004 (2014).
[44] V. Khachatryan *et al.* (CMS Collaboration), Eur. Phys. J. C **74**, 3076 (2014).
[45] V. S. Fadin, L. N. Lipatov, A. D. Martin, and M. Melles, Phys. Rev. D **61**, 094002 (2000).
[46] J. H. Kuhn, F. Metzler, A. A. Penin, and S. Uccirati, J. High Energy Phys. 06 (2011) 143.
[47] A. Denner and T. Hahn, Nucl. Phys. **B525**, 27 (1998).
[48] A. Denner and S. Dittmaier, Nucl. Phys. B, Proc. Suppl. **160**, 22 (2006).
[49] E. Accomando, A. Denner, and S. Pozzorini, J. High Energy Phys. 03 (2007) 078.
[50] T. Hahn and M. Perez-Victoria, Comput. Phys. Commun. **118**, 153 (1999).
[51] N. Blinov and D. E. Morrissey, J. High Energy Phys. 03 (2014) 106.
[52] A. Kusenko, P. Langacker, and G. Segre, Phys. Rev. D **54**, 5824 (1996).
[53] V. Barger, P. Huang, M. Ishida, and W. Y. Keung, Phys. Lett. B **718**, 1024 (2013).
[54] C. S. Lim, T. Inami, and N. Sakai, Phys. Rev. D **29**, 1488 (1984).
[55] M. Drees and K. Hagiwara, Phys. Rev. D **42**, 1709 (1990).
[56] S. Heinemeyer, W. Hollik, and G. Weiglein, Phys. Rep. **425**, 265 (2006).
[57] G. Aad *et al.* (ATLAS and CMS Collaborations), J. High Energy Phys. 08 (2016) 045.
[58] A. Djouadi, Phys. Rep. **457**, 1 (2008).
[59] A. Djouadi, Phys. Rep. **459**, 1 (2008).
[60] G. Aad *et al.* (ATLAS Collaboration), Phys. Rev. Lett. **113**, 141803 (2014).
[61] V. Khachatryan *et al.* (CMS Collaboration), Phys. Rev. Lett. **114**, 051801 (2015).
[62] E. Accomando, A. Ballestrero, A. Belhouari, and E. Maina, Phys. Rev. D **74**, 073010 (2006).

[63] J. Alwall, R. Frederix, S. Frixione, V. Hirschi, F. Maltoni, O. Mattelaer, H.-S. Shao, T. Stelzer, P. Torrielli, and M. Zaro, J. High Energy Phys. 07 (2014) 079.
[64] A. Denner, S. Dittmaier, and T. Hahn, Phys. Rev. D **56**, 117 (1997).
[65] B. Biedermann, A. Denner, and M. Pellen, arXiv: 1611.02951.
[66] P. Borel, R. Franceschini, R. Rattazzi, and A. Wulzer, J. High Energy Phys. 06 (2012) 122.
[67] A. Alboteanu, W. Kilian, and J. Reuter, J. High Energy Phys. 11 (2008) 010.
[68] W. Bernreuther and L. Chen, Phys. Rev. D **93**, 053018 (2016).
[69] C. Fleper, W. Kilian, J. Reuter, and M. Sekulla, Eur. Phys. J. C **77**, 120 (2017).
[70] F. Bishara, R. Contino, and J. Rojo, arXiv:1611.03860.
[71] K. Doroba, J. Kalinowski, J. Kuczmarski, S. Pokorski, J. Rosiek, M. Szleper, and S. Tkaczyk, Phys. Rev. D **86**, 036011 (2012).
[72] W. Kilian, T. Ohl, J. Reuter, and M. Sekulla, Phys. Rev. D **91**, 096007 (2015).
[73] W. Kilian, T. Ohl, J. Reuter, and M. Sekulla, Phys. Rev. D **93**, 036004 (2016).